universe

MDPI

Article

Mechanical Properties of Cometary Surfaces

Jens Biele [1,*], Jean-Baptiste Vincent [2] and Jörg Knollenberg [2]

[1] DLR—German Aerospace Center, RB-MUSC, 51147 Cologne, Germany
[2] DLR—German Aerospace Center, Institute for Planetary Research, 12489 Berlin, Germany
* Correspondence: jens.biele@dlr.de

Abstract: Mechanical properties, in particular, strength (tensile, shear, compressive) and porosity, are important parameters for understanding the evolution and activity of comets. However, they are notoriously difficult to measure. Unfortunately, neither Deep Impact nor other comet observations prior to Rosetta provided firm data on the strength of cometary material. This changed with the Rosetta mission and its detailed close observation data and with the landing(s) of Philae in 2014. There are already many articles and reviews in the literature that derive or compile many different strength values from various Rosetta and Philae data. In this paper, we attempt to provide an overview of the available direct and indirect data; we focus on comet Churyumov–Gerasimenko/67P but include a discussion on the Deep Impact strength results. As a prerequisite, we start by giving precise definitions of 'strength', discuss soil mechanics based on the Mohr–Coulomb 'law' of micro-gravity, and discuss bulk density and porosity, sintering, and the physics of the strength of a cohesive granular medium. We proceed by discussing the scaling of strength with the size and strain rate, which is needed to understand the observational data. We show how measured elastic properties and thermal (conductivity) data can be correlated with strength. Finally, a singular very high strength value is reviewed as well as some particularly small-strength values inferred from the bouncing motion of Philae, data from its collisions with the surface of the comet, and scratch marks it left, allegedly, on the surface close to its final resting site. The synthesis is presented as an overview figure of the tensile and compressive strength of cometary matter as a function of the size scale; conclusions about the size dependence and apparent natural variability of strength are drawn.

Keywords: comets; mechanical properties; strength; density; porosity; Churyumov–Gerasimenko; 67P

Citation: Biele, J.; Vincent, J.-B.; Knollenberg, J. Mechanical Properties of Cometary Surfaces. *Universe* **2022**, *8*, 487. https://doi.org/10.3390/universe8090487

Academic Editor: Ruisheng Zheng

Received: 5 July 2022
Accepted: 5 September 2022
Published: 15 September 2022

1. Introduction

The knowledge of the mechanical properties of cometary materials is important for several reasons. First, the origins matter in accretion mechanics (sticking vs. breaking up of dust agglomerates). Second, the dynamical and thermal evolution of a comet and, in particular, the observable physical processes (activity, impact, regolith transport), depending on the strength and porosity. For small bodies in general, mechanical properties are not only important for planetary defence, impact risk, and mitigation strategies, but also for asteroid mining.

The YORP effect changes the rotation state of a small body. In the case of spin-up, this may lead to a partial or total disruption; the critical rotation period for small asteroids rotating faster than the 'spin barrier' (period of 2.3 h for a typical bulk density of 2000 kgm^{-3}) requires some internal strength if the body is a rubble pile [1].

The thermal, mechanical, structural, and dielectric properties of cometary nuclei have been discussed in great detail by [2], and a whole chapter in the upcoming Comets III book is dedicated to material properties (Aurélie Guilbert-Lepoutre, priv. comm.).

In this mini review, we attempt to provide a critical overview of the available direct and indirect data; we focus (but not exclusively) on comet Churyumov–Gerasimenko/67P and in the summary, provide a synthesis of what is known about the mechanical properties of comets.

2. Materials and Methods

2.1. Definitions: Density, Porosity

One key descriptive variable for cometary matter is the extent to which the granular material (ices, refractories) fills the available space. This is commonly referred to as the packing fraction or packing density η, defined as the fraction of space occupied by particles. Within the geotechnical community, it is more common to report the complement $\varepsilon = (1 - \eta)$ called the void fraction or porosity [3]. We will use ε for porosity = void fraction, η for packing density or packing fraction, and ρ for the densities (grain density: material mass density excluding any pores). Macroporosity is defined as the volume of void space between the particles or constituents (which may have voids in the interior, i.e., microporosity) of a porous medium divided by the total volume. The bulk (total) porosity of a body with both micro- and macroporosity is not the sum of the two:

$$\begin{array}{l} \varepsilon_{bulk} = 1 - \frac{\rho_{bulk}}{\rho_{grain}} \\ \varepsilon_{Macro} = \frac{\varepsilon_{bulk} - \varepsilon_{micro}}{1 - \varepsilon_{micro}} \end{array} \quad (1)$$

Equation (1) is only valid for media made up of particles with identical microporosities. The general equation relating porosities and (average grain, bulk) densities is

$$\begin{array}{l} \varepsilon_{Macro} = 1 - \frac{\rho_{bulk}/\rho_{grain}}{1 - \sum_{i=1}^{m} \varepsilon_{micro,i} \mathrm{v}_i} \\ \sum \mathrm{v}_i = 1 \end{array} \quad (2)$$

The v_i are the volume fractions of particles with microporosity ε_i, given as a binned (size-sorted) histogram with m bins. Note that macroporosity can be further divided into intergranular porosity (between particles) and intragranular porosity (re-entrant surfaces on the exterior of particles) and that micropores can be divided into open pores and subgranular, closed pores [4]. This is important for gas transport through the porous medium.

The (macro)porosity of a random packing of equal-sized, non-cohesive spheres is within the dense and loose packing bounds, 36.5% [5] and ~42–44%, with the latter depending on friction and stress [6,7]. For granular media with a wide size distribution of particles, the macroporosity is lower than that of equal-sized spheres (compare Figure 1), whereas any (irregular) deviation from the spherical shape of the grains tends to increase porosity (for a semi-empirical model to calculate this see [8] and references therein). If the particles of a granular bed are cohesive, the porosity of the bed increases monotonically with the so-called granular Bond number Bo, the ratio of cohesive force (per contact) and weight:

$$Bo = \frac{F_{vdW}}{mg} = \frac{F_{vdW}}{\Pi \rho g d^3} \quad (3)$$

Here, g is the local gravity, m is the mass, ρ is the density, d is the diameter of a particle, and Π is a dimensionless shape factor of the order of 1 (0.52 for a sphere). There is a fairly universal empirical relation (e.g., [9,10]) between porosity and Bo, confirmed by DEM simulations. For example, a porosity of 75% (random packing, monodisperse) requires Bo~4000, which for typical comet conditions translates into a particle diameter of the order of 50 μm (using the van der Waals forces for rough particles calculated by [1]). However, almost arbitrarily, high porosities can exist (i.e., are mechanically stable in the gravity of the comet) if the particles are bonded, which leads us to the next section.

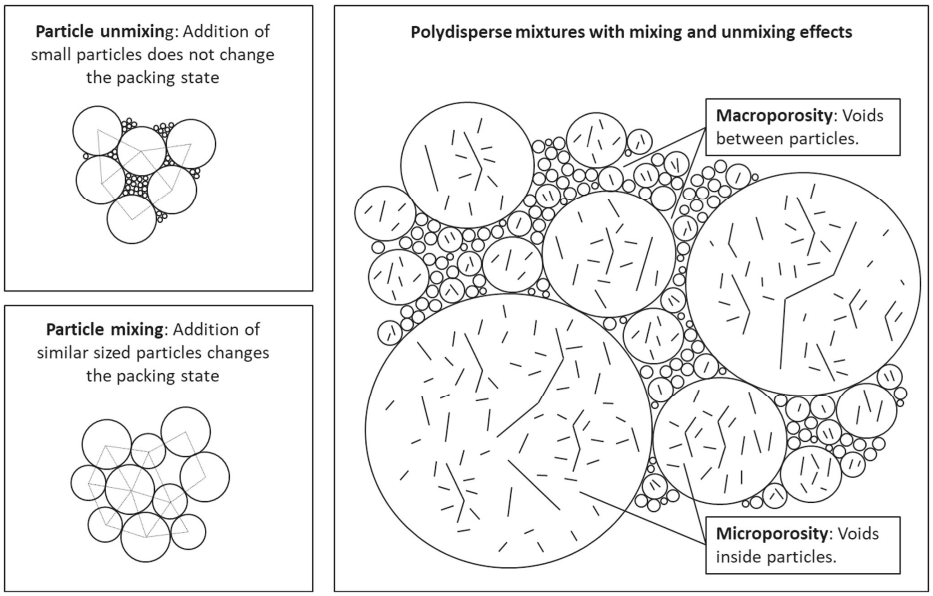

Figure 1. Porosity. (**Top left**): Illustration of particle unmixing for particles with strongly disparate diameters. As small particles are added to a system of larger particles, the larger particles resist being displaced and the packing state does not change. A similar effect occurs for the addition of very large particles. (**Bottom left**): Illustration of particle mixing for particles with similar diameters. As similar-sized particles are added to a system, particles can be displaced, thus changing the packing state. (**Right**): Illustration of the random packing structure of strongly polydisperse spheres. Compared to monodispersed configurations, porosity is reduced by the filling of void spaces. Macroporosity refers to the porosity generated by the void spaces between particles, whereas microporosity is caused by void spaces and cracks that formed inside individual particles.

2.2. Definition: Bonding

We have to distinguish between granular media, where the individual grains may experience friction/interlocking and cohesive (van der Waals) forces with their neighbours and 'bonded' (e.g., sintered) porous media, which typically form from the granular matter if the particle contacts form chemical or hydrogen bonds. There are various mechanisms possible to form strong bonds: cold- or hot-pressing, i.e., sintering involving solid diffusion; cold-welding (metals), or, more important for cometary matter, recondensing volatiles forming sinter necks preferentially around particle contacts. Bonded granular media are fundamentally different to granular matter: they have some mechanical 'competence' similar to a solid, cannot flow (just creep, at most), and their strength and thermal conductivity are very strong functions of the dimension of their bonds, scaling with the diameters of the sinter necks.

The theory of sintering in comets, i.e., by recondensing volatiles, is a complex field and has been described by various authors, e.g., [11,12]. To discuss sintering is beyond the scope of this paper, but one result is very important: even a small degree of sintering changes the mechanical (and thermal) properties drastically.

Note that there are two main kinds of sintering that relate to porosity: (1) no change in porosity—dependency of partial pressure of volatiles on the radius of curvature, molecules are transported from the same grain to its contact necks [13], (2) change in porosity if volatiles are coming from outside the sample volume and re-condense preferentially around the contact necks.

2.3. Definitions: Strength

By strength, we mean the ability of a material to withstand an applied load without failure (breaking) or (less important for brittle materials) plastic deformation >5%, expressed as a force per unit area, which corresponds to an energy per volume. For a schematic of

the behaviour of an elastoplastic medium when the load is compressive see Figure 2. Compressive strength is identified as the ultimate strength (catastrophic failure), tensile strength is identified analogously as the ultimate strength in tension (similar to cohesion), and shear strength is identified as the ultimate strength under a shearing load. For rather brittle materials as expected for cometary matter, the yield strength, ultimate strength, and breaking strength coincide at strains of <5%

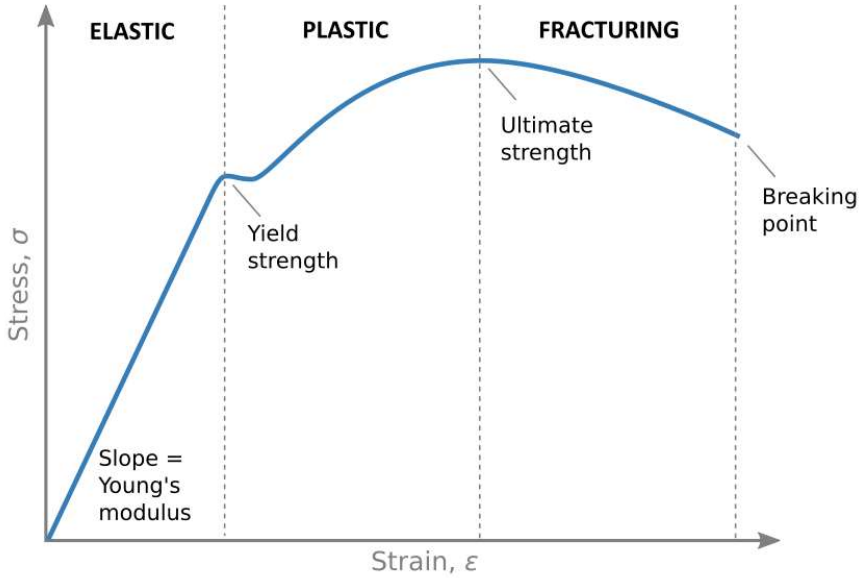

Figure 2. Schematic stress–strain diagram for an elastoplastic solid. A brittle solid typically shows just an approximately linear stress–strain curve up to failure, i.e., yield strength, ultimate strength, and breaking strength coincide at strains of <5%.

Different definitions of strength are adopted (or implied) in the literature and particular care is needed when comparing the results. For instance, cratering physics models include an 'effective strength' parameter that often depends on how the material equation of state and damage model are implemented rather than the actual properties of the object (see above). In the following paragraphs, we use the unqualified word *strength* to present the observations and models in general and we specify the type of strength (tensile σ_T, shear σ_S, or compressive $\sigma_{C)}$ when it is known unambiguously. As we showed above, the general approximation for granular or weakly bonded porous materials is that σ_C is typically at least one order of magnitude larger than σ_S and σ_T.

The compressive strength σ_C is uniquely measured by applying force along a certain axis until a predefined state of the sample (brittle failure or permanent deformation) is obtained. The force along the axis can be exerted on the sample either while perpendicular to this axis and the material is not confined—uniaxial (unconfined) compression—or the sample can be also confined in the perpendicular direction—triaxial compression. Almost all available data are on uniaxial compressive strength. In this paper, unless otherwise indicated, 'compressive strength' is uniaxial compressive strength.

Note that 'flexural strength', which is relevant for bending failure, e.g., for overhangs, is approximately equal to tensile strength (or smaller, if the surface under tension has more imperfections than the bulk material). 'Buckling' of a column of material is theoretically only dependent on Young's modulus for an elastic medium but for brittle materials, compressive failure is usually reached before any 'buckling' can be observed. In general, ductile materials or soils under high confining stress fail in shear, whereas brittle materials (most geologic materials, at least under low confining pressure) fail in tension. For the shear strength (=torsional strength) of geologic, in particular, granular materials, the normal (perpendicular) pressure has to be specified. We show in Section 2.3.1 that the

'strength' generally also depends on the strain rate and size of the specimen; therefore, the information on all these quantities needs to be given a meaningful strength value.

In cratering and impact physics, scaling laws are frequently applied [14,15] that use an "effective" strength that is not precisely defined. It is clear though that the outcome of an impact (real scale experiments: Deep Impact [16], Hayabusa 2 [17], DART [18,19]) can be very different depending on whether it takes place in a *strength* or *gravity regime*; strain rates are naturally orders of magnitude higher than for all other processes we regard here. Finally, there are also several engineering terms, such as (scratch, indentation) hardness, (fracture) toughness, wear resistance, etc., which we do not discuss here.

For common (terrestrial) rocks, the *compressive strength* is of the order of 10–300 MPa, and *tensile strength* and *shear strength* are 10 (tensile)–20 (shear) times smaller. The latter is true for almost all brittle materials Note that even for the commercial reference materials, the compressive or tensile strength for a given size and strain rate is known to scatter by up to a factor of 2 depending on the testing method/geometry [20] or 20–30% from specimen to specimen [21].

The penetration resistance (or (ultimate) bearing capacity/strength in soil mechanics or the semi-confined compressive strength) can be defined as the force per area of a pile (diameter d) driven quasi-statically into a semi-infinite often granular medium where the displaced matter either reduces porosity in the volume affected (which is of the order of d^3) or heaves up the surface around the intruder. It should not be confused with dynamic drag resistance, which scales as *(relative velocity)*^{2}.

For a homogenous, isotropic medium and a thin pile, the static penetration resistance per unit area should be (ideally) twice the uniaxial compressive strength for geometrical reasons of stress propagation [22]. It is important to note that it exists even in cohesionless granular matter with friction angle ϕ. Under microgravity, however, the cohesion term c (shear strength under zero normal load) is dominant, then bearing a capacity of $\approx N_c(\phi) \cdot c$, with $N_c(\phi)$ a unitless factor that is typically 20–50 for typical friction angles of $30° \pm 5°$ (see Section 2.3.3 and Figure 3 below and, e.g., [23,24]). Bearing strength is depth-dependent if there is a significant overburden pressure (such as on Earth) and obviously, the (triaxial = confined and to a lesser degree semi-confined) compressive strength of a granular medium must sharply increase once the random closed packing or "jammed" state has been reached.

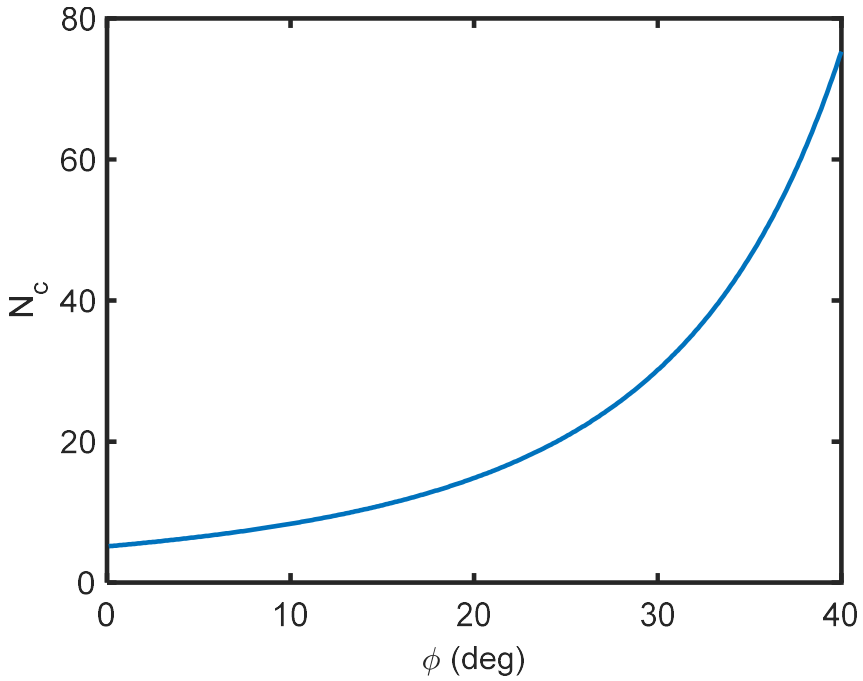

Figure 3. Bearing capacity factor N_c as a function of internal friction angle ϕ, from [25].

2.3.1. Strain Rate Dependence of Strength

Strain rate $\dot{s}$ is defined as the time derivative of (dimensionless) strain. A process can be called quasi-static if $\dot{s} <\approx 1$ is typically $<\approx 0.01$ 1/s. It is known that the compressive strength of brittle materials depends on the rate of deformation; the faster the deformation, the greater the measured strength values (note that ice *additionally* flows plastically at very low strain rates). All brittle solids, including geophysical and engineering materials, appear to follow a universal dependence of the compressive strength σ_c on the strain rate $\dot{s}$ with respect to the quasi-static compressive strength $\sigma_{c,0}$:

$$\begin{aligned} \sigma_c &= \sigma_{c,0}\left(1 + \dot{s}_*^{2/3}\right) \\ \dot{s}_* &= \dot{s}/\dot{s}_0 \end{aligned} \tag{4}$$

where $\dot{s}_0$ is a material constant of the order of 200 to 1000 s^{-1} for terrestrial rocks, ordinary chondrites, and concrete [26]. Thus, a rate effect of σ_c is expected for strain rates >200 s^{-1}, which is much higher than the strain rates of all Philae–comet contacts or of boulders falling from cliffs on 67P (<10 s^{-1}). At first glance, a significant effect would be expected for the Deep Impact cratering experiment [16] but this is not the case, as the hypervelocity crater scaling correlations are 'calibrated' with the quasi-static material strengths of the laboratory samples.

2.3.2. Size Dependence of Strength

The strength of (even slightly) consolidated materials also depends on the volume under stress; strength generally decreases with increasing size. The size effect is important if comparing local (dm to m-scale) strength with global comet nucleus strengths; it is predicted to disappear if the length scale is much smaller than a certain threshold D_0. The often-assumed linear elastic fracture mechanics (LEFM) size dependence of strength $\sim D^{-0.5}$ for brittle failure is not valid for all length scales D, and also not valid for granular non-bonded media.

The effective tensile strength in LEFM is given by (e.g., [27–30]):

$$\sigma_{eff} \propto D^{-3/(2\omega)} \tag{5}$$

Here, ω is the exponent for the power law flaw size distribution. Note that as the LEFM (Weibull) size effect is statistical, the effective strength σ_{eff} represents the average of the scattered individual values (although the size dependence on particle strength is systematic, the results of strength tests performed on particles of similar sizes may vary by up to one order of magnitude [29]). LEFM is very successful on large scales; Housen and Holsapple [27] combined observations of flaw sizes in terrestrial rocks, from millimetre-sized cracks in ~1–10 cm laboratory samples to ten-kilometre faults and fractures in the field, and suggested that $\omega \approx 3$ applies for rocks of all these scales.

A more realistic description of the scale dependence of strength has been given by [31] and is schematically depicted in Figure 4. Note that the LEFM $\sim 1/D^{1/2}$ dependence is the asymptote at large sizes, whereas below the characteristic size D_0, strength becomes independent of size (as long as D is larger than the scale of the intrinsic inhomogeneities of the material). D_0 is estimated, with the empirical constant λ calibrated with concrete as $D_0 = \lambda l \approx 40\ l$ [31,32], with l the inhomogeneity size of the inclusions in the material. The latter seems to be ~1 mm for common (L) meteorites [33,34], consistent with the size of large chondrules or CAIs, and might be ~3 mm or larger for the 'pebbles' imaged by the CIVA cameras at the 67P Abydos site [35].

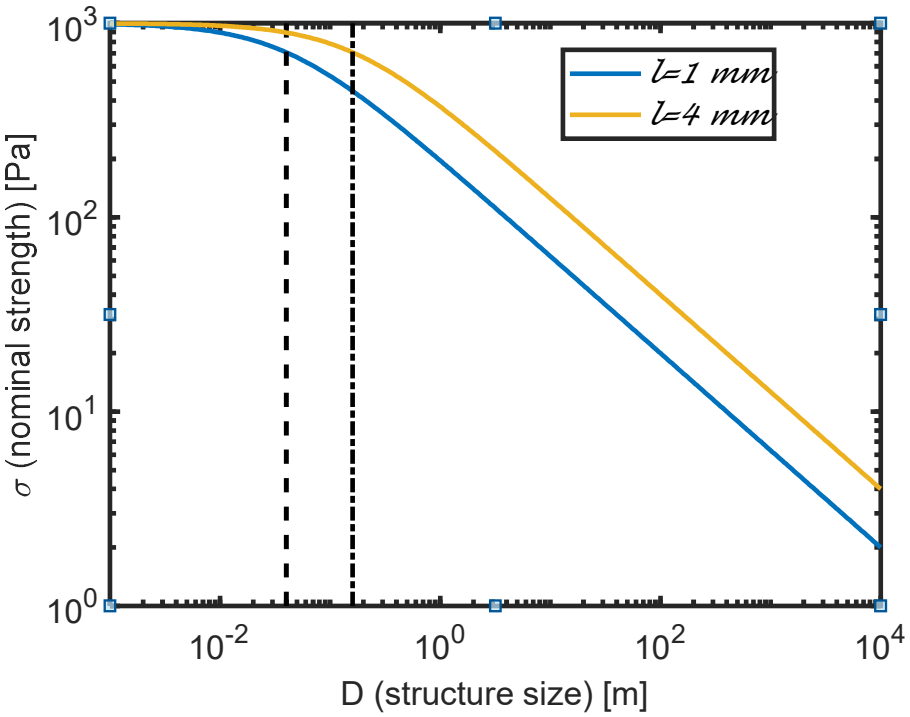

Figure 4. Size effect law [31] for quasi-brittle failures bridging the power law of plasticity (horizontal asymptote) and the power law of LEFM (inclined asymptote). The small-size asymptotic strength (compressive or tensile) has been arbitrarily set to 1000 Pa and l to 1 mm (blue curve) or 4 mm (yellow curve). These values could be roughly appropriate for the cometary material at 67P's Abydos site (see main text). The corresponding values of D_0, 40 mm and 160 mm, are indicated as vertical black dashed and dash-dotted lines, respectively.

2.3.3. Terminology of Soil Mechanics and Application to Micro-Gravity

It is useful to introduce the terms "cohesion" and "angle of friction". These refer to the Mohr–Coulomb (MC) failure criterion representing the plot ('linear failure envelope') that is obtained from a plot of the shear strength of a material versus the applied normal stress, as in Equation (6). It is a simplified mathematical model describing reasonably well the response of brittle materials, such as rocks or rubble piles, to shear stress as well as normal stress. The theory applies typically to materials for which the compressive strength far exceeds the tensile strength.

$$\sigma_s = p_n \tan\phi + c \tag{6}$$

where σ_s is the shear strength, p_n is the normal stress, c is the intercept of the failure envelope with the σ_s axis (i.e., shear strength at zero normal pressure), and ϕ is called the angle of internal friction. Compression is assumed to be positive. Note that the linearity implicit in the Mohr–Coulomb equation is just a convenient approximation and in reality, the $\sigma_s(p_n)$ relation is often curved, in particular, at a small p_n (e.g., [36]). Nevertheless, linear MC is the basis for engineering soil mechanics [37–40], which adopts the so-called limit equilibrium method to identify the ultimate bearing capacity of the ground. The general shear failure of the soil is determined as part of the analysed scenario in which multiple slip faces are generated. Note that the ultimate bearing capacity of the soil depends on the damage mode with large porosities or soft soil prone to produce punching shear failure (other modes are local shear failure and general shear failure) [38]. A large portion of terrestrial soil mechanics deals with the effects of pore water and groundwater, complications that we can neglect here; also, depth- and gravity-dependent terms (caused by the overburden pressure and 'upheaving') can often but not always be neglected in the micro-gravity environment of comets. Comet 67P has a typical surface gravity of 1.6×10^{-4} ms^{-2}, generating an overburden pressure of less than 0.1 Pa/m; the g-dependent

terms [23,41] create an additional 'bearing strength' of the order of 2 z [Pa/m] with depth z and 0.5 D [Pa/m], with the size D of the intruder.

Note that soil mechanics is not a precise theory. Depending on the detailed modelling of failure, the expressions, e.g., for the ϕ-dependent factors, such as N_c, vary by the order of 10%; other pre-factors depend on the shape of the 'foundation' and are of order unity but known only empirically to an accuracy of the order of 10%.

The angle of internal friction ϕ is typically a function of grain shape. Smooth, rounded grains may have ϕ lower than 25°, whereas jagged, spiky grains can lock together and permit values in excess of 35°. The angle relates to the angle of repose of a 'sandpile'; realistic values on planetary surfaces are probable in the 30°–35° range [41].

3. The Available Data

Before the Rosetta mission arrived at comet Churyumov–Gerasimenko in 2014, the range of bulk densities, porosities, and strengths for a comet was very uncertain [23,42,43]. Unfortunately, neither Deep Impact nor other comet observations seemed to provide firm data on the strength of cometary material. The few observational constraints available for comets and cometary meteoroids [23], as well as theoretical considerations and laboratory measurements [44] for weakly bound aggregates, led us to estimate the quasi-static tensile (or shear) strength of cometary material in the dm- to m-range as of the order of 1–10 kPa, whereas the compressive strength was estimated as of the order of 10–100 kPa with an uncertainty of at least one order of magnitude. The upper limit of compressive strength was estimated as 100 kPa (comet surface engineering model for the design of Philae, [43]).

Locally, higher strength values might occur ("crust", compacted ice). A tensile strength of 5 MPa for cold-sintered comet material was taken as a worst-case scenario in the design of the Philae lander anchoring harpoons [45–47].

Table 1 shows the typical strength values for these materials that could indicate the range of values to be expected on a comet.

Table 1. Strength of snow and firn ice as a function of density; adapted from [48,49]. Note that the experimental data scatter significantly around the average values shown here.

Material	Tensile Strength/kPa (Depth If Sintered from Top)	Comments	Ref.
Snow	0.3–2000	in air	[49]
H_2O ice, porous (73%), sintered	1000 (0...0.1 m) 100 (0.1...0.5 m) 500 (0.5...0.65 m) 1000 (>0.65 m)	ρ_0 = 261 kgm^{-3}, strongly sintered (compact ice crust of a few cm, below texture of well-sintered snow)	[24]
CO_2 ice, porous (48%)	2400 (crust) 200...500 (below)	CO_2 ice powder, sintered. ρ_0 = 806 kgm^{-3}	[24]
Solid ice	700–3000	−15 °C, increases moderately for lower temperatures	[49,50]

Water ice's mechanical and thermophysical properties are important because ice is the main volatile involved in sintering in cometary material.

The dependence of different strength measures for a temperature of about −15 °C on the density of porous ice is shown in Figure 5. It is evident that the small-scale strength in the relevant density range of 300–500 kg m^{-3} is of the order of 10–100 kPa. It should further be noted that the compressive strength shows a remarkable increase with decreasing temperatures [49,51,52], 4 times over the range from 0 °C to −40 °C, whereas the tensile strength is nearly independent of temperature [50]. Another source of experience comes from the KOSI (German for "comet simulation") experiments. Ref. [53] measured Young's modulus and the compressive strength (actually, penetration resistance, about a factor

~2 higher than σ_c) of ice–dust mixtures with high porosity at temperatures between 123 K and 253 K in laboratory experiments. The setup aimed at "simulating" possible cometary analogue material, i.e., solar heating from the top and sintering by recondensing volatiles. The KOSI and related experiments showed that the compressive strength and Young's modulus increase with decreasing temperature, decreasing dust content, and increasing density. Only very dense mixtures show an increase in compressive strength, similar to that of solid ice. Mixtures with bulk density ≤ 700 kgm^{-3} showed constant σ_c below ~230 K. The ratio of Young's modulus E and compressive strength σ_c was found to be ~100. Ref. [54] found a value of 20 kPa for their amorphous ice samples with a density of 250 kg m^{-3}.

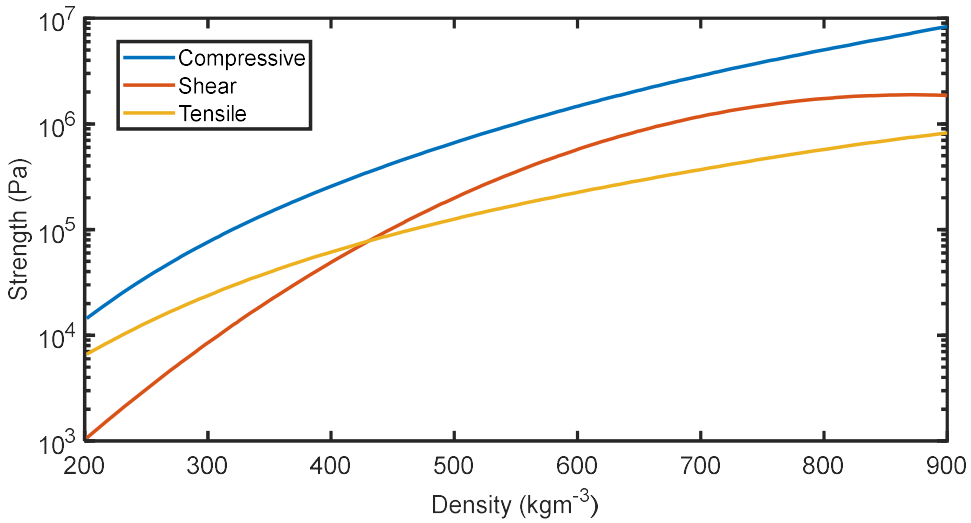

Figure 5. Strength of snow and firn ice as a function of density; adapted from [48,49]. Note that the experimental data scatter significantly around the average curves shown here.

4. Results from Space Missions (and Telescopic Observations)

4.1. Porosity

For most cometary nuclei, a high porosity (70–80%) is suggested; it has never been measured directly and has always been derived from the observed bulk densities and estimated or assumed composition. However, even precise global bulk densities exist only for comets that have been rendezvoused by spacecraft, and the global total porosity can only be inferred from the estimated global dust:ice mass ratio F and the composition of the ice(s), which is typically 75% amorphous water ice and 25% CO_2 ice with an average density of 958 ± 5 kgm^{-3}. The density of the refractories (the 'dust') is rather uncertain and the dust:ice ratio in the nucleus is extremely uncertain for cometary nuclei.

The nucleus material bulk density can be determined precisely for rendezvoused comets (mass from radio science divided by volume from shape model); however, it is difficult to determine at smaller scales. With knowledge of the bulk parameters only, it is also not possible to distinguish clearly between micro- and macro-porosity, though large voids in the nucleus of 67P can be excluded, based on gravity field data [55].

The Deep Impact experiment on comet 9P/Tempel 1 did enable a coarse estimate of the bulk density of 400 kg m^{-3} (200–1000 kg m^{-3}) from the dynamics of the impact ejecta [56].

For 67P, we have more constraints for porosity: using $\rho_{bulk} = (537.8 \pm 0.6)$ kgm^{-3} [57], the dust:ice mass ratio F = 1–7, a chondritic average grain density of the dust (2.27–3.69 g/cm^3 [58]), and the measured dielectric properties [59,60], the porosity seems to increase from 58% in the first meter to 75–86% below [2,60,61]. Note that F in the nucleus is very uncertain; it may be 1–7 [59] or 0–2.4 [62] or 0.03–2.4 [62] or $\geq$5 [63] or <2.3, with very wide margins [64].

The link between density and porosity assumes some of the other properties (composition, material densities [55]) and the relevant relations are (see also Figure 6)

$$\begin{aligned} w_{dust} &= \tfrac{F}{1+F} && \text{Dust mass fraction} \\ \rho_g &= \left[\tfrac{w_{dust}}{\rho_{dust}} + \tfrac{(1-w_{dust})}{\rho_{ices}}\right]^{-1} && \text{Average grain density} \\ \varepsilon_{t,b} &= 1 - \rho_{bulk}/\rho_g && \text{Total bulk porosity} \end{aligned} \tag{7}$$

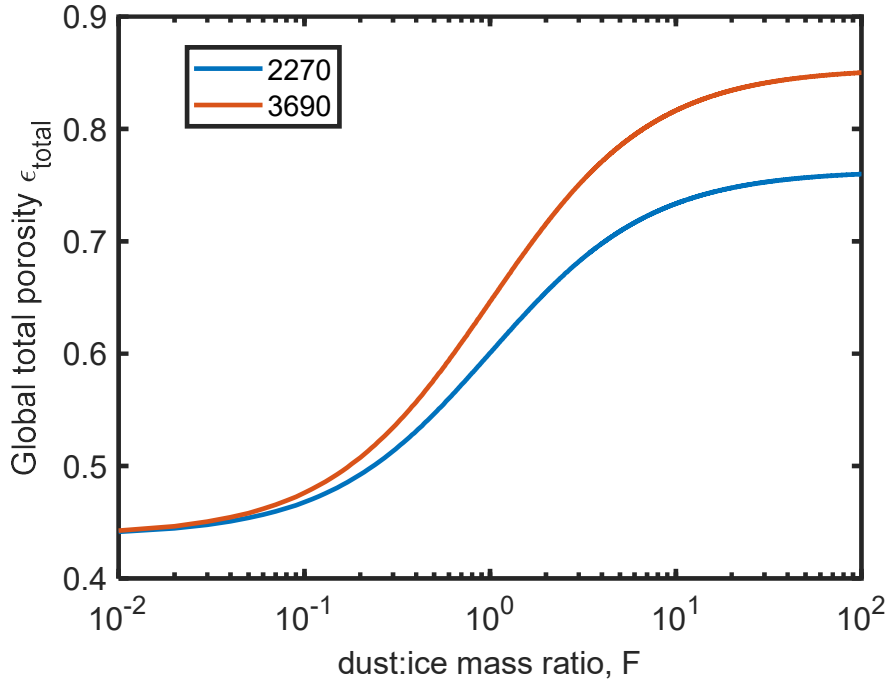

Figure 6. Global, total porosity of comet 67P vs. dust:ice mass ratio F. Parameter is the dust grain density in kgm^{-3}, i.e., the bounds of carbonaceous chondrite meteorites from [58]. The density of ice (actually a mix of various frozen volatiles after [60]) is assumed as (957.5 $\pm$ 4.5) kgm^{-3} and the global average bulk density as (537.8 $\pm$ 0.6) kg m^{-3} [57]; microporosity of both dust and ice is assumed to be 0. The dust:ice ratio in the nucleus is still debated (see main text).

4.2. Strength

This section summarizes the strength values obtained by space missions to comets. The numbers we report are not direct measurements as they would be done in controlled laboratory experiments, but they are typically upper or lower boundaries for strength derived from joint studies involving observations of physical processes, and our best theoretical understanding of the parameters controlling those processes. Because no mission could yet conduct dedicated strength measurements, the properties of cometary surfaces are typically determined from indirect observations such as morphological studies at different scales.

At the largest scale, i.e., the full nucleus of a few km, the tensile strength (now of the whole comet, not just the surface material) can be bracketed from two observations: cometary nuclei with known rotation rates and sizes (visited by spacecraft) do not break up at their current rotation rate but tidal forces have been observed to tear apart a comet. Those observations provide a lower and higher boundary to the strength of the bulk nucleus, respectively. Cometary nuclei must have a few Pa of tensile strength to resist rotational break up [65] but no more than 100 Pa (tidal stress in disruption events such as the encounter of comet Shoemaker–Levy 9 with Jupiter [66] or the disruption of the sun-grazing comets, [67].

On scales of 10 to 100 m, cliffs and spires are prominent features of cometary topography that can be as tall as several hundred meters, with overhangs that sometimes collapse.

The height of these cliffs and in general, all gravitational slopes steeper than the material angle of repose (or internal friction angle), provides a direct constraint on the *tensile strength*. Reports from several comets show a lower limit of a few Pa [68–71].

For comet 67P, Groussin et al. [70] analysed the collapsed cliff overhangs observed from orbit. Assuming that they collapsed under their own weight and not due to other causes, they derived a compressive (maybe rather tensile, for bending failure?) strength of the consolidated material that most likely is in the range of 30–150 Pa (overhangs, scale 5 m) with an upper limit of 1.5 kPa (surface materials, 10 cm scale) and a compressive strength of the collapsed structures <11.6 kPa (1 m scale). The strength of the consolidated material was also estimated by analysing the terrain characteristics of the steep cliffs, where the material is exposed on the surface. Based on these observations, the tensile strength of the material is in the range of 1.5 to 100 Pa, the shear strength is in a range of ~13 to $\geq$30 Pa, and the compressive strength is in a range of 30 to 150 Pa and possibly up to 1.5 kPa [72]. Thomas et al., 2015 [73], were among the first to estimate the tensile strength of some overhangs on 67P, resulting in values of 10–20 Pa for 10 m size. Although all these values are extremely low compared to rocks on Earth (typical tensile strength is in the MPa range), it is sufficient for cliffs to survive in the very low-gravity environment of a comet.

In the same scale range, the effective strength of cometary material could be inferred through studies of the Deep Impact crater, which report an upper limit of 12 kPa [16,74]. More precisely, from scaling relations for impact models of the temporal evolution of the morphology of the DI cratering event, Richardson et al. [56] estimated a bulk tensile strength for the excavated upper layers of the comet of 1–10 kPa. Housen and Holsapple [74] have argued that the estimates of Richardson et al. may be low by an order of magnitude, that is, ~100–1000 Pa.

Below the 10 m scale, comets such as 67P are covered with boulders [75,76] that may have fallen from the aforementioned cliffs or may have been ejected by cometary activity from one area of the nucleus falling back on another. Rosetta observed such processes in several instances, reporting objects up to several 10 s of meters in size travelling 100 m or further without breaking up [77,78]. It was estimated that boulders must have a compressive strength σ_c > 200–2000 Pa in order to withstand the impact stress. This range is compatible with the Deep Impact results [42,79].

We note that most cometary boulders appear to be made of consolidated materials, whereas most "airfall" areas (as in the Agilkia area of 67P, see [73]) seem to consist of granular matter with very small tensile strength but still ~1–10 kPa compressive strength [78,80–82].

At smaller scales (1–50 cm), our best knowledge of the surface material strength comes from the multiple touchdowns of Philae on comet 67P and its scientific operations in the Agilkia (apparently granular) and Abydos (apparently well-consolidated material) sites.

Upon its first landing at Agilkia, Philae did not succeed in damping all of its velocity and bounced back, leaving behind clear imprints (craters) of its contacts (not of the 3 feet!) in the regolith and excavating ~200 kg of material [80]. This provided a unique opportunity to study a low-velocity impact in a semi-controlled test as mass, velocity, and material properties of the 'projectile' were perfectly known. The authors of [80–82] used this information and data provided by the onboard accelerometers to derive a compressive strength of the regolith in the kilopascal range. A similar range of values was found in the Hapi region, where a 10 m large falling boulder bounced several times on the surface, leaving clear imprints in the regolith [78].

The collisions of Philae after its first touchdown until its final rest could be rather well reconstructed and the coefficients of restitution (tangential, normal) could be estimated [83]. Heinisch et al. [84] attempted to reconstruct the attitude of Philae during its bouncing flight [85] and derived mechanical strength values from the inferred interactions of specific parts of the lander structure with the collision surfaces. They derived an overall upper limit of *compressive strength* of ~800 Pa (including all uncertainties) for 'consolidated material' but locally derived 'upper limit' values of 8 ± 7, 73 ± 77, 147 ± 77, and 399 ± 393 Pa. We do not,

however, consider these values as *upper* limits for two reasons: first, they contain a dynamic penetration resistance term of at least 12–60 Pa (see below) and second, they critically depend on applying the correct interacting area of Philae's structure in the interactions. The latter is based on a Philae attitude vs. time model [85], which, to the best of our knowledge, was not checked for consistency with the (Euler) equations of motion of Philae's complex rotation and on a simplified shape model of the comet near the contact points, which means that the real contacts due to small-scale roughness on the comet's surface may have resulted in completely different, smaller contact areas. Partly sliding contacts (the case to be expected, in general) would explain the long contact durations without necessarily meaning the deep (~0.5 m) intrusion of parts of the Philae structure into the comet surface.

We now discuss some analyses that significantly stand out from the general picture.

4.2.1. Philae's Collisions: The Putative Ultra-Soft Cometary Material

After O'Rourke et al. [86], the final collision of Rosetta's lander Philae with an 'outcrop' of a few meters in diameter at the Abydos site and the subsequently claimed damage to that object, seemed to show that some boulders are extremely fragile. The authors, under the main working assumption that certain features of images almost 19 months apart were caused by Philae ("scratches") and assuming various cross-sections or lengths that could not be measured on the said images, reported a compressive strength of $\leq$12 Pa, which as an *upper* limit value is so low that its tensile and shear strength must be less than ~1 Pa. Maybe more importantly, such a material is very likely inconsistent with the transmission and the velocity of the sound waves observed by the Philae CASSE experiment at the Abydos site. Assume, for instance, a compressive strength σ_C of only 100 Pa, an (unrealistically large) ratio E/σ_C = 1000, and a Poisson number in the range 0–0.4, the velocity of Rayleigh waves must be 7.5–9 m/s, that is, one order of magnitude below the CASSE lower limit. Even the smallest measured shear wave velocities in the lunar regolith are larger (>25 m/s, [87]), and a non-negligible strength is necessary so that the material can transmit shear (or Rayleigh) waves.

For granular (not cemented) media with bulk density ρ, the dynamic intrusion resistance for velocity v can be written as $\frac{1}{2}\rho C_D v^2$, where C_D is ~4 for low-velocity impacts [88,89]; using C_D = 2, ρ = 538 kg/m^3, and v = 0.15 m/s (Philae's velocity just before final collision, ([80], Table S3), we obtain at contact a ~24 Pa penetration resistance. This is not a strength.

The quasi-static compressive strength σ_C would come on top of any measured dynamic penetration resistance; we can estimate it according to soil mechanics as $\sigma_C \approx c\, N_c(\phi)$, with $N_c(30^\circ)$ = 30 (30° might be typical for planetary regolith grains [41]); the cohesion c, which has the same order of magnitude as tensile strength, can be roughly estimated using Rumpf's equation [90,91], $c \approx (1-\varepsilon)/\varepsilon \times F_{vdW}/d^2$. Assuming $F_{vdW} \approx 1$ nN (from [1]) and a grain diameter d of 12 μm [64], then c ≈ 2 Pa and the compressive strength ($\propto 1/d^2$) would still be ~70 Pa, albeit extremely uncertain (we know neither the mean size of load-bearing 'grains' nor the roughness parameters necessary to calculate the van der Waals cohesion). The important point is that the very low tensile strength according to the Rumpf equation excludes the slightest bonding by, e.g., sintering, which is not consistent with the other observations of consolidated material at the Abydos site.

Even if the assumptions in O'Rourke et al. [86] are correct and one boulder displays an extremely low value of compressive strength, it should be noted that these results are not necessarily representative of cometary material in other regions. For instance, as discussed above, El Maarry et al. [77] and Vincent et al. [78] reported on boulders larger than 10 m travelling over tens of meters (possibly ejected by outbursts) and surviving the journey. This indicates strength values that must be larger than what is inferred by [86]. Vincent et al. [78] derived a minimum compressive strength in the range of 230–2000 Pa for boulders in the Hapi region.

4.2.2. The Abydos Site of 67P: Review of the Putative Hard Material

Some experiments on Philae can provide data about the mechanical properties of the nucleus surface at Abydos. These are mostly from MUPUS, the thermal and mechanical properties probe consisting of a 32 cm-long penetrator driven by an electromagnetic hammer mechanism on top (see Figure 7), anchor sensors, and an infrared radiometer [92], and SESAME [93], an experiment suite consisting of a dust sensor (DIM), a permittivity probe (PP) for measuring electrical properties, and CASSE (comet acoustic surface sounding experiment), with its accelerometers and ultrasonic sources located in Philae's landing gear feet.

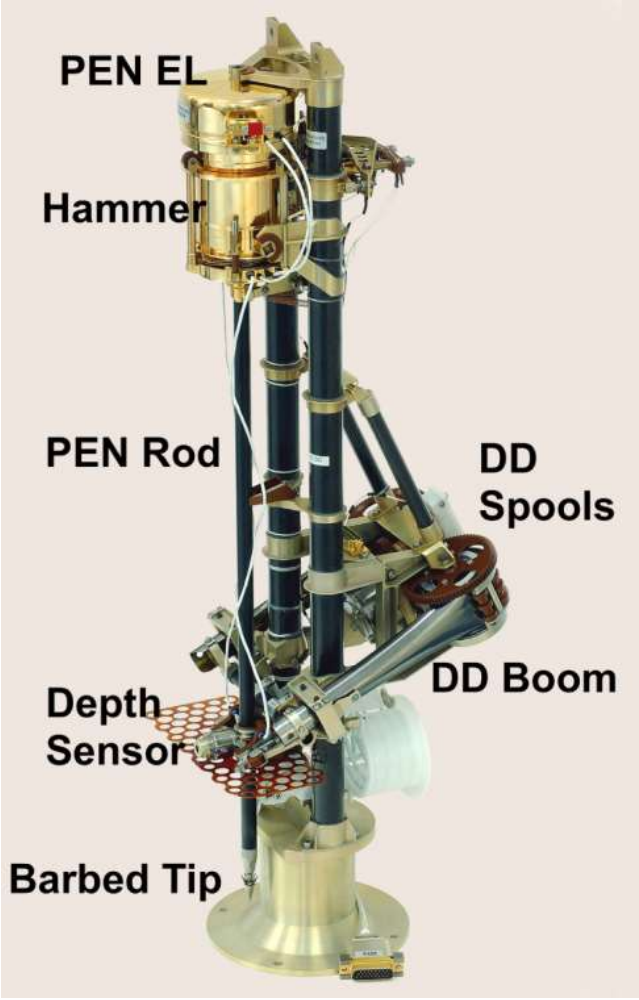

Figure 7. The MUPUS PEN with the deployment device in the stowed position on the lander (cruise configuration). From top to bottom, the figure shows the front-end electronics PEN-EL, the hammer mechanism, the PEN rod in which the temperature sensors are implemented, the deployment device spools and boom, the depth sensor, and the barbed tip of the PEN. The PEN is mounted to two struts that are bolted onto the top of the APX housing. The red perforated plate is a SESAME PP electrode and is not part of the MUPUS package. The diameter of the PEN is 10 mm, and the diameter of the hammer head is ~70 mm. Image courtesy of J. Knollenberg.

At the final landing site, the MUPUS penetrator did not succeed in breaching through the surface, suggesting the material hardened to a compressive strength of $\sigma_c > 2$ MPa [22], at first being unconstrained to even higher values. This value was based on the observed bouncing of the PEN on the spot after an initial downward movement of 27 mm (as indicated by the depth sensor) and the known penetration performance from the pre-launch experiments together with the assumption that the PEN tip was hammering on the surface of the comet. Unfortunately, no independent proof, e.g., images, exists to

confirm that the tip indeed interacted with the ground. It is easy to overlook that several caveats to this conclusion were made by the authors in the Supplementary Materials of their publication. In addition, there might be another possibility that could affect the strength value derived from the non-penetration. Because of the non-nominal working of the hammer at the highest energy level (EL = 4), Spohn et al. used the stroke energy of EL = 3 (which worked nominally) for their derivation of the strength. Ground tests at this energy level had shown successful penetration into a material of 2.1 MPa but at a very low penetration rate (~0.2 mm per 4-stroke sequence). Only 8 such 4-stroke hammering sequences at this energy level were performed. Pre-launch testing had also shown that the initial penetration was most difficult because anchoring of the tip by its barbs was necessary to avoid rebound. To achieve this, the PEN needs to hammer several times on nearly the same spot until the required depth of a few mm is reached. It seems plausible that the probably rough and steep sloped surface of the boulder [94], together with the low penetration rate, may have prevented the initial penetration of the tip. In this case, the lower limit for the compressive strength would reduce to 0.58 MPa (±30%).

A possible problem (as already mentioned by [22], in the Supplementary Materials) with the derived lower strength limit conclusion is the assumption that the PEN interacts with the surface at its tip. However, it cannot be excluded that there is another explanation for the absence of penetration progress, namely the blocking of the PEN hammer head by a protrusion of the nearby boulder. That is, the PEN tip was 'hammering into vacuum', whereas the head hammered against the protrusion 'ledge'.

In this case, a crude estimate of the necessary boulder strength can be given by $\sigma > E/V$, where E is the stroke energy and V is the effective volume. The lower part of the PEN hammer head is approximately a cylinder with an equivalent radius of R_H = 27 mm. Approximating the effective volume [38] by a half cylinder of the same radius R_H (because the PEN tube prevents more than one-half of the area from interacting with the boulder) and a height of H = 2 R_H and using a hammer energy of E = 2.2 J (at EL = 3) and a nominal efficiency of 25% from the conversion of electrical to mechanical energy [95], results in a lower limit of $\sigma > 9$ kPa. In this case, the strength σ can be considered a combination of shear and tensile strength. For brittle materials (note that the brittle behaviour of the boulders at Abydos is indicated by the many fractures that were observed by the CIVA camera [35]), the compressive strength is typically a factor of 5–20 higher than the tensile strength, which results in a lower limit of compressive strength of $\sigma_c > 45$ kPa.

Another source of information about the mechanical properties of the comet surface stems from the SESAME/CASSE listening to the MUPUS hammer strokes [87]. CASSE clearly detected seismic Rayleigh-type surface waves generated by the MUPUS hammering that were travelling through the comet to the detectors located in the feet of Philae. Assuming a flat surface, the arrival times of the waves could be converted to a Rayleigh wave speed of $v_R = 132.5 +/- 17.6$ m/s. Using very conservative assumptions about the error bounds (three sigmas), the Poisson number (0–0.416), the possible density range of the cometary surface layer (515–1635 kg m^{-3}), and the geometry (wave path lengths), Knapmeyer et al. [87] deduced Young's modulus in the range of 7.2 MPa < E < 980 MPa. For the relevant depth scale, the surface waves of CASSE are mostly determined by the first one-third of the wavelength with $\lambda = v_R/f$ with f~250 Hz–1 kHz, thus a depth of a few (2–3) dm [87]. Furthermore, the observed frequency-dependent dispersion of the Rayleigh waves indicates a transition to less rigid material below. An even harder thin layer on top cannot be excluded, but it cannot be thicker than a few cm otherwise, it would have been visible in the CASSE data.

In our opinion, some of the assumptions made in [85] are over-conservative, especially the factor of 3 for the ratio of the true wave path length to Euclidean distance. Applying a two-sigma lower limit (common in metrology) for v_R and using a maximum factor of 1.5 for the ratio of the true wave path length to Euclidean distance (which seems to be compatible with the 3D reconstruction of the local geometry below the lander by ROLIS [96]), the plausible range for Young's modulus would reduce to 12.8 < E < 192 MPa.

Furthermore, the thermal inertia $TI = \sqrt{k\, c_P\, \rho_{bulk}}$ at Abydos estimated from the measurements by the radiometer MUPUS-TM can also be used to derive clues about the mechanical properties of the surface at Abydos. The MUPUS TM field-of-view is predominantly filled by the same boulder that probably interacted with the PEN and transmitted the seismic waves to the Philae + Y-foot. It has to be noted that both cameras on Philae do not show any indication of the presence of a dust layer on the surface of the boulders [35,96], thus it seems plausible (cf. [97]) that the thermal properties of the boulder interior (down to several cm) were sampled by MUPUS TM. The authors in [22] derived a value for the thermal inertia of 85+/−35 J m^{-2} K^{-1} s$^{-1/2}$, which was later corrected to TI > 120 J m^{-2} K^{-1} s$^{-1/2}$ [2] and further constrained to <180 J m^{-2} K^{-1} s$^{-1/2}$ [20]. Using the density range given above, a temperature of 110 K, a refractory/ice mass ratio of between 1 and 5, and the specific heat values for CI carbonaceous chondrites and water ice [98], one finds a thermal conductivity of the mixture of about 0.06 W m^{-1} K^{-1}, bounded by 0.02 and 0.10 Wm^{-1} K^{-1}. This is about one order of magnitude higher than that of smooth terrains (dusty, smooth units such as Imhotep, Hatmehit, etc.) with a very low thermal inertia (10–30 J K^{-1} m^{-2} s$^{-1/2}$ [2,99]). It is important to note that at the very low temperature of Abydos of T = 110 K the radiative contribution of even large millimetre-sized grains would be below 10^{-3} W m^{-1} K^{-1} (using the theory of Sakatani [100]) and can be neglected. The relatively high values of thermal conductivity observed by MUPUS-TM at the Abydos site can only be explained by some sort of cementation (e.g., by sintering of water ice and formation of sinter necks between the grains) that binds the grains together. The relevant size scale is given by the diurnal thermal skin depth, s

$$s = \sqrt{\kappa P/\pi \rho c_p} = \frac{\Gamma}{\rho c_P}\sqrt{\frac{P}{\pi}}$$

Here, P is the diurnal period, κ is the thermal conductivity) of ~5 cm, as TI values are influenced by the first ~3 skin depths.

For a random packing of identical, isotropic, and homogeneous spheres with shear modulus μ and Poisson's ratio ν, the bulk elastic parameters can then be related to those in a porous medium following the approach of Digby [101]. In Hertzian contact theory, two identical spheres have a circular contact area of radius rc depending on the confining pressure and Young's modulus of the sphere material. In an extension of the Hertz contact model, Digby assumes that the contact area between two spheres contains a small, concentric area of radius $r < r$c, where the spheres are firmly bonded, that is, remain in contact even without confining pressure. He obtains the effective Lamé parameters of the packing. We take the adhesive region as a model for a sintering neck between two particles and consider the case without confining pressure, where $r \equiv r$c. The point is that according to the conventional theory of effective thermal conductivity k (without radiative parte) of a granular bed, k is also proportional to rc.

Under these circumstances, the thermal conductivity k of the bulk can be related to the effective Young's modulus of the porous boulder by derivation (see [102]):

$$E_{Digby} = \frac{\pi}{8}\frac{k}{k_g}E_g \tag{8}$$

where k_g *i*s the thermal conductivity of the solid grain and E_g is the Young's modulus of the solid.

Digby's theory is strictly applicable for a single component system where the bounds (cement) between the spherical grains have the same elastic properties as the grains. It seems reasonable that the bulk elastic properties are mostly determined by the cementing material. Therefore, we choose the appropriate values of ice at 110 K for the grain properties, k_g = 5.9 W m^{-1} K^{-1} [103,104] and E_g = 10.3 GPa [51,105]. Then a thermal inertia of 120 J m^{-} K^{-1} s$^{-1/2}$ can be converted by Equation (8) to $E \approx E_{Digby}$ = 14–69 MPa. The lower

limit for Young's modulus derived from the thermal properties fits well with the lower bound derived from the seismic wave analysis.

Because thermal conductivity, elastic modulus, and strength for porous consolidated materials are governed mainly by the bonds between grains, it is natural to assume that correlations between these properties exist. From the results of [53], which we discussed above, one finds a ratio of E/σ_c~100. A similar value can be deduced from the results of [106] on artificial snow. For natural snow, the review of Mellor [48] indicates a higher E/σ_c of about 500 on average, which is comparable to E/σ_c for compact rocks [107]. For ~1 cm specimens of compacted powders, the experimental work of Sun [108] found a range of E/σ_c of 347 (compacted plastic material powder, porosity 9–27%) to 893 (compacted brittle material powder, porosity 40–50%). We use the range of E/σ_c = 100–500 for our conversion from Young's modulus to the compressive strength of the Abydos boulders resulting in 28 kPa < σ_c < 690 kPa from the thermal inertia data.

One might ask where, in this correlation between the elastic modulus and compressive strength, is the size dependence of the latter. The answer is that the empirical conversion factors are valid for typical laboratory samples of a size of 1–10 cm.

From the CASSE data alone, we have for compressive strength a lower limit of ~26 kPa and a rather uncertain upper limit of the order of 2 MPa (size scale 20–30 cm).

For the case discussed above where the MUPUS pen tip did not touch the surface, this range is further constrained to >45–690 kPa (both 5 cm scales). If it did but initial penetration did not succeed, the consequence is a lower limit for the compressive strength of 580 kPa (see above) on a scale of 10 mm; if we assume that the LEFM scaling still holds in this range, then the >580 kPa at 10 mm is equivalent to >260 kPa at a 5 cm scale; if not, at most the 580 kPa also applies at the 5 cm scale.

The final synthesis range for the Abydos site is thus 28 kPa–690 kPa on the 5–30 cm scale. Abydos is a rather special place—it is a cold trap because it is very poorly illuminated by the Sun and the average surface temperature is lower than in many other places, leading to unusually strong ice redeposition and sintering.

5. Conclusions

In Figure 8, we summarize the data on the strength of cometary materials discussed here; strength vs. size scale in double-logarithmic axes.

We have re-analysed the data for the apparently exceptional 67P Abydos site, where originally [22], a lower limit of several MPa for compressive strength was suggested. Our revised value for compressive strength is 28–690 kPa on the 5–30 cm scale, possibly representing the most competent material on the comet, potentially with a reduced porosity [60] compared to the average 70–80%.

We find that cometary material seems to follow the general expected trend that shows an increase in strength with decreasing scale, the $\propto d^{-0.5}$ scaling being at least not implausible; small grains are stronger than boulders, which are themselves stronger than large topographic features such as cliffs or the nucleus itself.

However, we also note that at any scale, the strength values span at least 2 orders of magnitude, and potentially more than 4 orders of magnitude. Part of this span must be due to the intrinsic differences between the material considered in various studies (airfall vs consolidated, ice-rich vs ice-poor, fraction of organic content, degree of sintering, etc.), which are mostly unknown. Furthermore, from the combination of data with many different underlying methods and looking at the spread at a given scale, we believe that inhomogeneity on many scales is the norm rather than the exception.

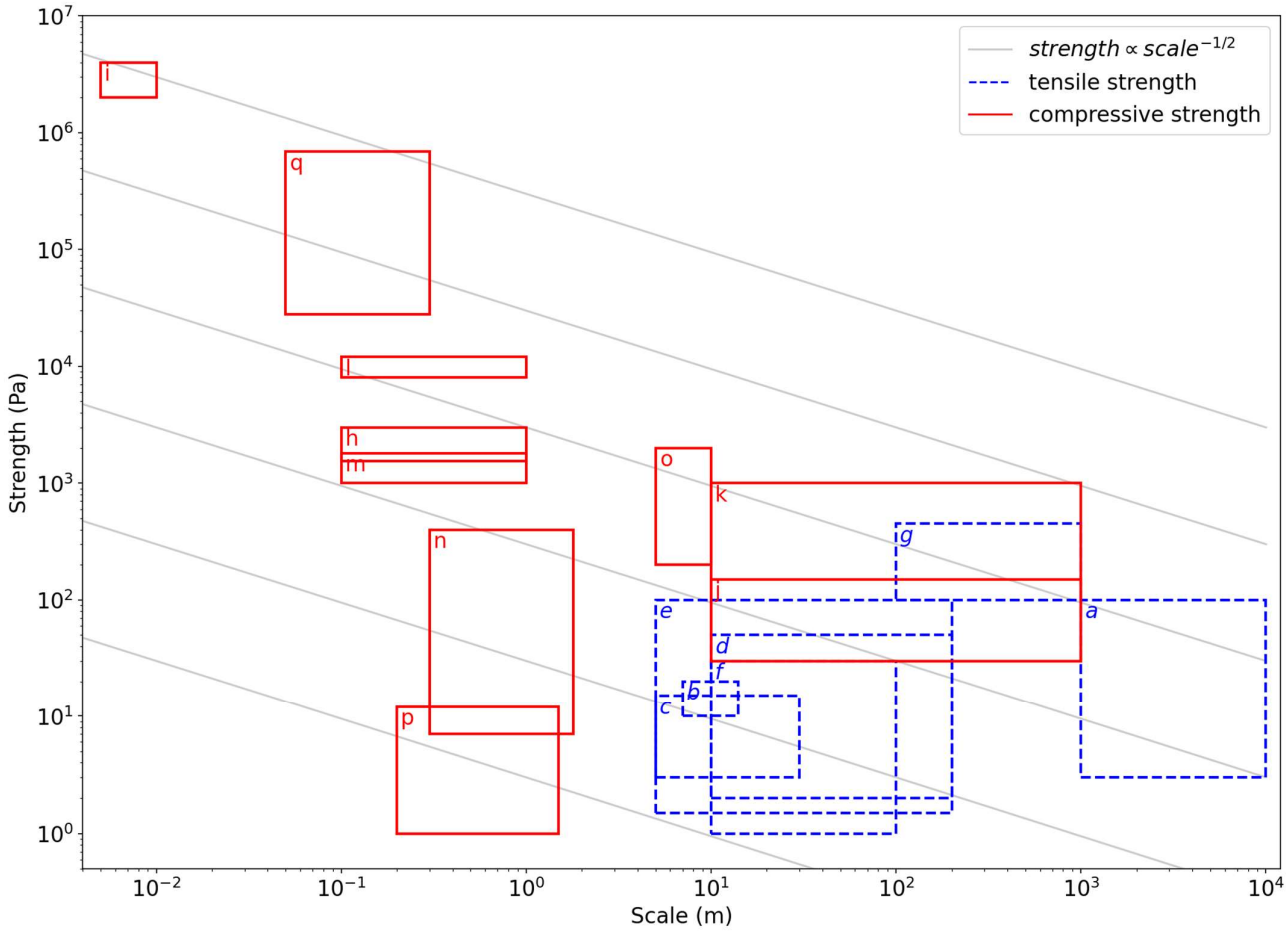

Figure 8. Summary of tensile and compressive strength for cometary materials from this work and the previously published literature. Each box represents a domain of scale/strength from a specific study. The thin gray lines in the background illustrate the typical qualitative relationship between strength and scale. References: (a) Biele + 2009 [23], (b) Thomas + 2015 [73], (c) Grousssin + 2015 [70], (d) Vincent + 2015,2017 [68,69], (e) Basilevsky + 2016 [72], (f) Attree + 2017 [71], (g) Matonti + 2019 [109], (h) Biele + 2015 [80], (i) Spohn + 2015 [22], (j) Grousssin + 2015 [70], (k) Basilevsky + 2016 [72], (l) Möhlmann + 2018 [110], (m) Roll + 2016 [81,82]. (n) Heinisch + 2019 [84], (o) Vincent + 2019 [78], (p) O'Rourke + 2020 0 [86], (q) this study.

In a nutshell, the strength values for the same size vary over 1 or 2 orders of magnitude (depending on the degree of bonding) from the median values, which very roughly could be written for non-granular material as a function of characteristic size scale D, as $\sigma_C \cong 10^3\,[\mathrm{Pa\,m^{1/2}}]/\sqrt{D/\mathrm{m}}$, and $\sigma_T \cong 10^2\,[\mathrm{Pa\,m^{1/2}}]/\sqrt{D/\mathrm{m}}$. Saturation of strength is predicted for $D \ll 0.04$ m but cannot be inferred from the data here.

Supplementary Materials: The following supporting information can be downloaded at: https://www.mdpi.com/article/10.3390/universe8090487/s1.

Author Contributions: Conceptualization, J.B. and J.-B.V.; Methodology, J.B.; Validation, J.B., J.-B.V. and J.K.; Writing—Original Draft Preparation, J.B.; Writing—Review and Editing, J.B., J.-B.V. and J.K.; Visualization, J.-B.V. All authors have read and agreed to the published version of the manuscript.

Funding: This research received no external funding.

Institutional Review Board Statement: Not applicable.

Informed Consent Statement: Not applicable.

Acknowledgments: We gratefully acknowledge helpful discussions with Stephan Ulamec (DLR).

Conflicts of Interest: The authors declare no conflict of interest.

References

1. Persson, B.; Biele, J. On the stability of spinning asteroids. *Tribol. Lett.* **2022**, *70*, 1–19. [CrossRef]
2. Groussin, O.; Attree, N.; Brouet, Y.; Ciarletti, V.; Davidsson, B.; Filacchione, G.; Fischer, H.-H.; Gundlach, B.; Knapmeyer, M.; Knollenberg, J. The thermal, mechanical, structural, and dielectric properties of cometary nuclei after Rosetta. *Space Sci. Rev.* **2019**, *215*, 29. [CrossRef]
3. Daniels, K.E. Rubble-pile near Earth objects: Insights from granular physics. In *Asteroids*; Springer: Berlin/Heidelberg, Germany, 2013; pp. 271–286.
4. Heiken, G.; Vaniman, D.; French, B.M. *Lunar Sourcebook-A User's Guide to the Moon*; Cambridge University Press: Cambridge, UK, 1991; p. 736.
5. Scott, G.; Kilgour, D. The density of random close packing of spheres. *J. Phys. D Appl. Phys.* **1969**, *2*, 863. [CrossRef]
6. Onoda, G.Y.; Liniger, E.G. Random loose packings of uniform spheres and the dilatancy onset. *Phys. Rev. Lett.* **1990**, *64*, 2727–2730. [CrossRef]
7. Jerkins, M.; Schröter, M.; Swinney, H.L.; Senden, T.J.; Saadatfar, M.; Aste, T. Onset of Mechanical Stability in Random Packings of Frictional Spheres. *Phys. Rev. Lett.* **2008**, *101*, 018301. [CrossRef]
8. Grott, M.; Biele, J.; Michel, P.; Sugita, S.; Schröder, S.; Sakatani, N.; Neumann, W.; Kameda, S.; Michikami, T.; Honda, C. Macroporosity and grain density of rubble pile asteroid (162173) Ryugu. *J. Geophys. Res. Planets* **2020**, *125*, e2020JE006519. [CrossRef]
9. Kiuchi, M.; Nakamura, A.M. Corrigendum to "Relationship between regolith particle size and porosity on small bodies" [*Icarus* 239 (2014) 291–293]. *Icarus* **2015**, *248*, 221. [CrossRef]
10. Kiuchi, M.; Nakamura, A.M. Relationship between regolith particle size and porosity on small bodies. *Icarus* **2014**, *239*, 291–293. [CrossRef]
11. Thomas, H. Untersuchung der Festigkeit Poröser Eis-Mineral-Körper Kometarer Zusammensetzung. Master's Thesis, Universität zu Köln, Köln, Germany, 1992.
12. Molaro, J.L.; Choukroun, M.; Phillips, C.B.; Phelps, E.S.; Hodyss, R.; Mitchell, K.L.; Lora, J.M.; Meirion-Griffith, G. The microstructural evolution of water ice in the solar system through sintering. *J. Geophys. Res. Planets* **2019**, *124*, 243–277. [CrossRef]
13. Kossacki, K.J.; Köinle, N.I.; Kargl, G.; Steiner, G. The influence of grain sintering on the thermoconductivity of porous ice. *Planet. Space Sci.* **1994**, *42*, 383–389. [CrossRef]
14. Holsapple, K.A.; Housen, K.R. Momentum transfer in asteroid impacts. I. Theory and scaling. *Icarus* **2012**, *221*, 875–887. [CrossRef]
15. Housen, K.R.; Sweet, W.J.; Holsapple, K.A. Impacts into porous asteroids. *Icarus* **2018**, *300*, 72–96. [CrossRef]
16. A'Hearn, M.F.; Belton, M.J.S.; Delamere, W.A.; Kissel, J.; Klaasen, K.P.; McFadden, L.A.; Meech, K.J.; Melosh, H.J.; Schultz, P.H.; Sunshine, J.M.; et al. Deep Impact: Excavating Comet Tempel 1. *Science* **2005**, *310*, 258–264. [CrossRef]
17. Watanabe, S.; Tsuda, Y.; Yoshikawa, M.; Tanaka, S.; Saiki, T.; Nakazawa, S. Hayabusa2 mission overview. *Space Sci. Rev.* **2017**, *208*, 3–16. [CrossRef]
18. Cheng, A.F.; Rivkin, A.S.; Michel, P.; Atchison, J.; Barnouin, O.; Benner, L.; Chabot, N.L.; Ernst, C.; Fahnestock, E.G.; Kueppers, M. AIDA DART asteroid deflection test: Planetary defense and science objectives. *Planet. Space Sci.* **2018**, *157*, 104–115. [CrossRef]
19. Rivkin, A.S.; Chabot, N.L.; Stickle, A.M.; Thomas, C.A.; Richardson, D.C.; Barnouin, O.; Fahnestock, E.G.; Ernst, C.M.; Cheng, A.F.; Chesley, S. The double asteroid redirection test (DART): Planetary defense investigations and requirements. *Planet. Sci. J.* **2021**, *2*, 173. [CrossRef]
20. Knollenberg, J. *Re-Analysis of MUPUS-TM Thermal Inertia for Abydos*; DLR PF: Berlin, Germany, 2020; *Unpublished work*.
21. Rüsch, H. *Statistische Analyse der Betonfestigkeit*; Deutscher Ausschuss für Stahlbeton: Berlin, Germany, 1969.
22. Spohn, T.; Knollenberg, J.; Ball, A.J.; Banaszkiewicz, M.; Benkhoff, J.; Grott, M.; Grygorczuk, J.; Hüttig, C.; Hagermann, A.; Kargl, G.; et al. Thermal and mechanical properties of the near-surface layers of comet 67P/Churyumov-Gerasimenko. *Science* **2015**, *349*, aab0464. [CrossRef]
23. Biele, J.; Ulamec, S.; Richter, L.; Knollenberg, J.; Kührt, E.; Möhlmann, D. The putative mechanical strength of comet surface material applied to landing on a comet. *Acta Astronaut.* **2009**, *65*, 1168–1178. [CrossRef]
24. Kömle, N.I.; Ball, A.J.; Kargl, G.; Keller, T.; Macher, W.; Thiel, M.; Stöcker, J.; Rohe, C. Impact penetrometry on a comet nucleus—Interpretation of laboratory data using penetration models. *Planet. Space Sci.* **2001**, *49*, 575–598. [CrossRef]
25. Craig, R.F. *Craig's Soil Mechanics*; CRC Press: Boca Raton, FL, USA, 2004.
26. Ramesh, K.; Hogan, J.D.; Kimberley, J.; Stickle, A. A review of mechanisms and models for dynamic failure, strength, and fragmentation. *Planet. Space Sci.* **2015**, *107*, 10–23. [CrossRef]
27. Housen, K.R.; Holsapple, K.A. Scale effects in strength-dominated collisions of rocky asteroids. *Icarus* **1999**, *142*, 21–33. [CrossRef]
28. Bryson, K.L.; Ostrowski, D.R.; Blasizzo, A. Meteorite flaws and scaling for atmospheric entry. *Planet. Space Sci.* **2018**, *164*, 85–90. [CrossRef]
29. Weibull, W. A statistical theory of strength of materials. *Ingeniörs Vetenskaps. Akad.* **1939**, *151*, 1–45.
30. Trustrum, K.; Jayatilaka, A.D.S. Applicability of Weibull analysis for brittle materials. *J. Mater. Sci.* **1983**, *18*, 2765–2770. [CrossRef]
31. Bažant, Z.P. Size effect on structural strength: A review. *Arch. Appl. Mech.* **1999**, *69*, 703–725. [CrossRef]

32. Bažant, Z.P.; Yu, Q. Universal size effect law and effect of crack depth on quasi-brittle structure strength. *J. Eng. Mech.* **2009**, *135*, 78–84. [CrossRef]
33. Pohl, L. *The Physical Properties of Asteroids*; University of Central Florida: Orlando, FL, USA, 2020.
34. Pohl, L.; Britt, D.T. Strengths of meteorites—An overview and analysis of available data. *Meteorit. Planet. Sci.* **2020**, *55*, 962–987. [CrossRef]
35. Poulet, F.; Lucchetti, A.; Bibring, J.-P.; Carter, J.; Gondet, B.; Jorda, L.; Langevin, Y.; Pilorget, C.; Capanna, C.; Cremonese, G. Origin of the local structures at the Philae landing site and possible implications on the formation and evolution of 67P/Churyumov-Gerasimenko. *Mon. Not. R. Astron. Soc.* **2016**, *462*, S23–S32. [CrossRef]
36. García-Triñanes, P.; Luding, S.; Shi, H. Tensile strength of cohesive powders. *Adv. Powder Technol.* **2019**, *30*, 2868–2880. [CrossRef]
37. Reissner, H. Zum Erddruckproblem. In Proceedings of the First International Congress for Applied Mechanics, Delft, The Netherlands, 22–26 April 1924; pp. 295–311.
38. Terzaghi, K.; Mesri, G.; Peck, R.B. *Soil Mechanics in Engineering Practice*; Wiley: Hoboken, NJ, USA, 1996.
39. Terzaghi, K. *Theoretical Soil Mechanics*; John Wiley and Sons Inc.: New York, NY, USA, 1943; Volume 314.
40. Meyerhof, G. The ultimate bearing capacity of foudations. *Geotechnique* **1951**, *2*, 301–332. [CrossRef]
41. Lorenz, R.D. Titan's surface bearing strength: Contact force models for the Dragonfly rotorcraft lander. *Planet. Space Sci.* **2022**, *214*, 105449. [CrossRef]
42. Biele, J.; Ulamec, S.; Richter, L.; Kührt, E.; Knollenberg, J.; Möhlmann, D. The Strength of Cometary Surface Material: Relevance of Deep Impact Results for Philae Landing on a Comet. In *Deep Impact as a World Observatory Event: Synergies in Space, Time, and Wavelength*; Springer: Berlin/Heidelberg, Germany, 2009; pp. 285–300.
43. Rosetta Lander Mission Analysis Working Group. *Comet Surface Engineering Model*; RO-ESC-RP-5006; ESA: Noordwijk, The Netherlands, 1999.
44. Blum, J.; Schräpler, R.; Davidsson, B.J.; Trigo-Rodriguez, J.M. The physics of protoplanetesimal dust agglomerates. I. Mechanical properties and relations to primitive bodies in the solar system. *Astrophys. J.* **2006**, *652*, 1768. [CrossRef]
45. Biele, J.; Ulamec, S. Capabilities of Philae, the Rosetta Lander. *Space Sci. Rev.* **2007**, *138*, 275–289. [CrossRef]
46. Biele, J.; Ulamec, S.; Feuerbacher, B.; Rosenbauer, H.; Mugnolo, D.; Moura, D.; Bibring, J.P. Current status and scientific capabilities of the ROSETTA Lander payload. *Adv. Space Res.* **2002**, *29*, 1199–1208. [CrossRef]
47. Kömle, N.I.; Ball, A.J.; Kargl, G.; Stöcker, J.; Thiel, M.; Jolly, H.S.; Dziruni, M.; Zarnecki, J.C. Using the anchoring device of a comet lander to determine surface mechanical properties. *Planet. Space Sci.* **1997**, *45*, 1515–1538. [CrossRef]
48. Mellor, M. A review of basic snow mechanics. In Proceedings of the Grindelwald Symposium, International Symposium of Snow Mechanics, Grindelwald, Switzerland, 1–5 April 1974; pp. 251–291.
49. Petrovic, J. Review mechanical properties of ice and snow. *J. Mater. Sci.* **2003**, *38*, 1–6. [CrossRef]
50. Litwin, K.L.; Zygielbaum, B.R.; Polito, P.J.; Sklar, L.S.; Collins, G.C. Influence of temperature, composition, and grain size on the tensile failure of water ice: Implications for erosion on Titan. *J. Geophys. Res.* **2012**, *117*, E08013. [CrossRef]
51. Schulson, E.M.; Duval, P. *Creep and Fracture of Ice*; Cambridge University Press: Cambridge, UK, 2009.
52. Schulson, E. The structure and mechanical behavior of ice. *JOM* **1999**, *51*, 21–27. [CrossRef]
53. Jessberger, H.; Kotthaus, M. Compressive strength of synthetic comet nucleus samples. In Proceedings of the Physics and Mechanics of Cometary Materials, Munster, Germany, 9–11 October 1989.
54. Bar-Nun, A.; Laufer, D. First experimental studies of large samples of gas-laden amorphous "cometary" ices. *Icarus* **2003**, *161*, 157–163. [CrossRef]
55. Pätzold, M.; Andert, T.; Hahn, M.; Asmar, S.W.; Barriot, J.P.; Bird, M.K.; Häusler, B.; Peter, K.; Tellmann, S.; Grün, E.; et al. A homogeneous nucleus for comet 67P/Churyumov–Gerasimenko from its gravity field. *Nature* **2016**, *530*, 63–65. [CrossRef]
56. Richardson, J.E.; Melosh, H.J.; Lisse, C.M.; Carcich, B.J.I. A ballistics analysis of the Deep Impact ejecta plume: Determining Comet Tempel 1's gravity, mass, and density. *Icarus* **2007**, *191*, 176–209. [CrossRef]
57. Pätzold, M.; Andert, T.P.; Hahn, M.; Barriot, J.-P.; Asmar, S.W.; Häusler, B.; Bird, M.K.; Tellmann, S.; Oschlisniok, J.; Peter, K. The Nucleus of comet 67P/Churyumov-Gerasimenko—Part I: The global view—nucleus mass, mass-loss, porosity, and implications. *Mon. Not. R. Astron. Soc.* **2019**, *483*, 2337–2346. [CrossRef]
58. Britt, D.; Yeomans, D.; Housen, K.; Consolmagno, G. Asteroid density, porosity, and structure. In *Asteroids III*; The University of Arizona: Tucson, AZ, USA, 2002.
59. Kofman, W.; Herique, A.; Barbin, Y.; Barriot, J.-P.; Ciarletti, V.; Clifford, S.; Edenhofer, P.; Elachi, C.; Eyraud, C.; Goutail, J.-P. Properties of the 67P/Churyumov-Gerasimenko interior revealed by CONSERT radar. *Science* **2015**, *349*, aab0639. [CrossRef] [PubMed]
60. Brouet, Y.; Levasseur-Regourd, A.C.; Sabouroux, P.; Neves, L.; Encrenaz, P.; Poch, O.; Pommerol, A.; Thomas, N.; Kofman, W.; Le Gall, A.; et al. A porosity gradient in 67P/C-G nucleus suggested from CONSERT and SESAME-PP results: An interpretation based on new laboratory permittivity measurements of porous icy analogues. *Mon. Not. R. Astron. Soc.* **2016**, *462*, S89–S98. [CrossRef]
61. Herique, A.; Kofman, W.; Zine, S.; Blum, J.; Vincent, J.-B.; Ciarletti, V. Homogeneity of 67P/Churyumov-Gerasimenko as seen by CONSERT: Implication on composition and formation. *Astron. Astrophys.* **2019**, *630*, A6. [CrossRef]

62. Marschall, R.; Markkanen, J.; Gerig, S.-B.; Pinzón-Rodríguez, O.; Thomas, N.; Wu, J.-S. The dust-to-gas ratio, size distribution, and dust fall-back fraction of comet 67p/Churyumov-Gerasimenko: Inferences from linking the optical and dynamical properties of the inner comae. *Front. Phys.* **2020**, *8*, 227. [CrossRef]
63. Fulle, M.; Blum, J.; Rotundi, A.; Gundlach, B.; Güttler, C.; Zakharov, V. How comets work: Nucleus erosion versus dehydration. *Mon. Not. R. Astron. Soc.* **2020**, *493*, 4039–4044. [CrossRef]
64. Choukroun, M.; Altwegg, K.; Kührt, E.; Biver, N.; Bockelée-Morvan, D.; Drążkowska, J.; Hérique, A.; Hilchenbach, M.; Marschall, R.; Pätzold, M. Dust-to-gas and refractory-to-ice mass ratios of comet 67P/Churyumov-Gerasimenko from Rosetta observations. *Space Sci. Rev.* **2020**, *216*, 1–38. [CrossRef]
65. Davidsson, B.J.R. Tidal Splitting and Rotational Breakup of Solid Biaxial Ellipsoids. *Icarus* **2001**, *149*, 375–383. [CrossRef]
66. Asphaug, E.; Benz, W. Size, Density, and Structure of Comet Shoemaker-Levy 9 Inferred from the Physics of Tidal Breakup. *Icarus* **1996**, *121*, 225–248. [CrossRef]
67. Klinger, J.; Espinasse, S.; Schmidt, B. Some considerations on cohesive forces in sun-grazing comets. In *Physics and Mechanics of Cometary Materials*; Hunt, J.J., Guyenne, T.D., Eds.; ESA Special Publication: Noordwijk, The Netherlands, 1989; Volume 302, pp. 197–200.
68. Vincent, J.-B.; Bodewits, D.; Besse, S.; Sierks, H. Large heterogeneities in comet 67P as revealed by active pits from sinkhole collapse. *Nature* **2015**, *523*, 63–66. [CrossRef]
69. Vincent, J.-B.; Hviid, S.F.; Mottola, S.; Kührt, E.; Kuehrt, E.; Preusker, F.; Scholten, F.; Keller, H.U.; Oklay, N.; de Niem, D.; et al. Constraints on cometary surface evolution derived from a statistical analysis of 67P's topography. *Mon. Not. R. Astron. Soc.* **2017**, *469*, S329–S338. [CrossRef]
70. Groussin, O.; Jorda, L.; Auger, A.-T.; Kührt, E.; Gaskell, R.; Capanna, C.; Scholten, F.; Preusker, F.; Lamy, P.; Hviid, S.; et al. Gravitational slopes, geomorphology, and material strengths of the nucleus of comet 67P/Churyumov-Gerasimenko from OSIRIS observations. *Astron. Astrophys.* **2015**, *583*, A32. [CrossRef]
71. Attree, N.; Groussin, O.; Jorda, L.; Nébouy, D.; Thomas, N.; Brouet, Y.; Kührt, E.; Preusker, F.; Scholten, F.; Knollenberg, J.; et al. Tensile strength of 67P/Churyumov-Gerasimenko nucleus material from overhangs. *Astron. Astrophys.* **2018**, *611*, A33. [CrossRef]
72. Basilevsky, A.T.; Krasil'nikov, S.S.; Shiryaev, A.A.; Mall, U.; Keller, H.U.; Skorov, Y.V.; Mottola, S.; Hviid, S.F. Estimating the strength of the nucleus material of comet 67P Churyumov-Gerasimenko. *Sol. Syst. Res.* **2016**, *50*, 225–234. [CrossRef]
73. Thomas, N.; Sierks, H.; Barbieri, C.; Lamy, P.L.; Rodrigo, R.; Rickman, H.; Koschny, D.; Keller, H.U.; Agarwal, J.; A'Hearn, M.F. The morphological diversity of comet 67P/Churyumov-Gerasimenko. *Science* **2015**, *347*, aaa0440. [CrossRef]
74. Holsapple, K.A.; Housen, K.R. A crater and its ejecta: An interpretation of Deep Impact. *Icarus* **2007**, *187*, 345–356. [CrossRef]
75. Pajola, M.; Vincent, J.-B.; Güttler, C.; Lee, J.-C.; Bertini, I.; Massironi, M.; Simioni, E.; Marzari, F.; Giacomini, L.; Lucchetti, A.; et al. Size-frequency distribution of boulders $\geq$7 m on comet 67P/Churyumov-Gerasimenko. *Astron. Astrophys.* **2015**, *583*, A37. [CrossRef]
76. Pajola, M.; Oklay, N.; La Forgia, F.; Giacomini, L.; Massironi, M.; Bertini, I.; El-Maarry, M.R.; Marzari, F.; Preusker, F.; Scholten, F.; et al. Aswan site on comet 67P/Churyumov-Gerasimenko: Morphology, boulder evolution, and spectrophotometry. *Astron. Astrophys.* **2016**, *592*, A69. [CrossRef]
77. El-Maarry, M.R.; Groussin, O.; Thomas, N.; Pajola, M.; Auger, A.-T.; Davidsson, B.; Hu, X.; Hviid, S.F.; Knollenberg, J.; Güttler, C.; et al. Surface changes on comet 67P/Churyumov-Gerasimenko suggest a more active past. *Science* **2017**, *355*, 1392–1395. [CrossRef]
78. Vincent, J.-B.; Birch, S.; Hayes, A.; Zacny, K.; Oklay, N.; Cambianica, P. Bouncing boulders on comet 67P. In Proceedings of the EPSC-DPS Joint Meeting 2019, Geneva, Switzerland, 15–20 September 2019; p. EPSC-DPS2019-2502.
79. Richardson, J.E.; Jay Melosh, H. An examination of the Deep Impact collision site on Comet Tempel 1 via Stardust-NExT: Placing further constraints on cometary surface properties. *Icarus* **2013**, *222*, 492–501. [CrossRef]
80. Biele, J.; Ulamec, S.; Maibaum, M.; Roll, R.; Witte, L.; Jurado, E.; Munoz, P.; Arnold, W.; Auster, H.U.; Casas, C.; et al. The Landing(s) of Philae and Inferences on Comet Surface Mechanical Properties. *Science* **2015**, *349*, aaa9816. [CrossRef] [PubMed]
81. Roll, R.; Witte, L. ROSETTA lander Philae: Touch-down reconstruction. *Planet. Space Sci.* **2016**, *125*, 12–19. [CrossRef]
82. Roll, R.; Witte, L.; Arnold, W. ROSETTA lander Philae–soil strength analysis. *Icarus* **2016**, *280*, 359–365. [CrossRef]
83. Jurado, E.; Martin, T.; Canalias, E.; Blazquez, A.; Garmier, R.; Ceolin, T.; Gaudon, P.; Delmas, C.; Biele, J.; Ulamec, S.; et al. Rosetta lander Philae: Flight Dynamics analyses for landing site selection and post-landing operations. *Acta Astronaut.* **2016**, *125*, 65–79. [CrossRef]
84. Heinisch, P.; Auster, H.U.; Gundlach, B.; Blum, J.; Güttler, C.; Tubiana, C.; Sierks, H.; Hilchenbach, M.; Biele, J.; Richter, I.; et al. Compressive strength of comet 67P/Churyumov-Gerasimenko derived from Philae surface contacts. *Astron. Astrophys.* **2019**, *630*, A2. [CrossRef]
85. Heinisch, P.; Auster, H.-U.; Richter, I.; Hercik, D.; Jurado, E.; Garmier, R.; Güttler, C.; Glassmeier, K.-H. Attitude reconstruction of ROSETTA's Lander PHILAE using two-point magnetic field observations by ROMAP and RPC-MAG. *Acta Astronaut.* **2016**, *125*, 174–182. [CrossRef]
86. O'Rourke, L.; Heinisch, P.; Blum, J.; Fornasier, S.; Filacchione, G.; Van Hoang, H.; Ciarniello, M.; Raponi, A.; Gundlach, B.; Blasco, R.A.; et al. The Philae lander reveals low-strength primitive ice inside cometary boulders. *Nature* **2020**, *586*, 697–701. [CrossRef]

87. Knapmeyer, M.; Fischer, H.H.; Knollenberg, J.; Seidensticker, K.J.; Thiel, K.; Arnold, W.; Faber, C.; Möhlmann, D. Structure and elastic parameters of the near surface of Abydos site on comet 67P/Churyumov-Gerasimenko, as obtained by SESAME/CASSE listening to the MUPUS insertion phase. *Icarus* **2018**, *310*, 165–193. [CrossRef]
88. Sunday, C.; Murdoch, N.; Wilhelm, A.; Drilleau, M.; Zhang, Y.; Tardivel, S.; Michel, P. The influence of gravity on granular impacts-II. A gravity-scaled collision model for slow interactions. *Astron. Astrophys.* **2022**, *658*, A118. [CrossRef]
89. Faug, T. Macroscopic force experienced by extended objects in granular flows over a very broad Froude-number range. *Eur. Phys. J. E* **2015**, *38*, 34. [CrossRef]
90. Rumpf, H. The strength of granules and agglomerates. In Proceedings of the Agglomeration—Proceedings of the First International Symposium on Agglomeration, Philadelphia, PA, USA, 12–14 April 1961; pp. 379–418.
91. Bika, D.G.; Gentzler, M.; Michaels, J.N. Mechanical properties of agglomerates. *Powder Technol.* **2001**, *117*, 98–112. [CrossRef]
92. Spohn, T.; Seiferlin, K.; Hagermann, A.; Knollenberg, J.; Ball, A.J.; Banaszkiewicz, M.; Benkhoff, J.; Gadomski, S.; Gregorczyk, W.; Grygorczuk, J. MUPUS—A thermal and mechanical properties probe for the Rosetta lander Philae. *Space Sci. Rev.* **2007**, *128*, 339–362. [CrossRef]
93. Seidensticker, K.J.; Möhlmann, D.; Apathy, I.; Schmidt, W.; Thiel, K.; Arnold, W.; Fischer, H.-H.; Kretschmer, M.; Madlener, D.; Péter, A. Sesame—An experiment of the rosetta lander philae: Objectives and general design. *Space Sci. Rev.* **2007**, *128*, 301–337. [CrossRef]
94. Ulamec, S.; O'Rourke, L.; Biele, J.; Grieger, B.; Andrés, R.; Lodiot, S.; Muñoz, P.; Charpentier, A.; Mottola, S.; Knollenberg, J. Rosetta Lander-Philae: Operations on comet 67P/Churyumov-Gerasimenko, analysis of wake-up activities and final state. *Acta Astronaut.* **2017**, *137*, 38–43. [CrossRef]
95. Grygorczuk, J.; Banaszkiewicz, M.; Seweryn, K.; Spoin, T. MUPUS insertion device for the Rosetta mission. *J. Telecommun. Inf. Technol.* **2007**, *1*, 50–53.
96. Schröder, S.; Mottola, S.; Arnold, G.; Grothues, H.-G.; Jaumann, R.; Keller, H.; Michaelis, H.; Bibring, J.-P.; Pelivan, I.; Koncz, A. Close-up images of the final Philae landing site on comet 67P/Churyumov-Gerasimenko acquired by the ROLIS camera. *Icarus* **2017**, *285*, 263–274. [CrossRef]
97. Biele, J.; Kührt, E.; Senshu, H.; Sakatani, N.; Ogawa, K.; Hamm, M.; Grott, M.; Okada, T.; Arai, T. Effects of dust layers on thermal emission from airless bodies. *Prog. Earth Planet. Sci.* **2019**, *6*, 48. [CrossRef]
98. Biele, J.; Grott, M.; Zolensky, M.E.; Benisek, A.; Dachs, E. The specific heat capacity of astro-material I: Review of theoretical concepts, materials and techniques. *Int. J. Thermophys.* **2022**, *43*, 143. [CrossRef]
99. Schloerb, F.P.; Keihm, S.; Von Allmen, P.; Choukroun, M.; Lellouch, E.; Leyrat, C.; Beaudin, G.; Biver, N.; Bockelée-Morvan, D.; Crovisier, J. MIRO observations of subsurface temperatures of the nucleus of 67P/Churyumov-Gerasimenko. *Astron. Astrophys.* **2015**, *583*, A29. [CrossRef]
100. Sakatani, N.; Ogawa, K.; Iijima, Y.; Arakawa, M.; Honda, R.; Tanaka, S. Thermal conductivity model for powdered materials under vacuum based on experimental studies. *AIP Adv.* **2017**, *7*, 015310. [CrossRef]
101. Digby, P. The effective elastic moduli of porous granular rocks. *J. Appl. Mech.* **1981**, *48*, 803–808. [CrossRef]
102. Grott, M.; Knollenberg, J.; Hamm, M.; Ogawa, K.; Jaumann, R.; Otto, K.A.; Delbo, M.; Michel, P.; Biele, J.; Neumann, W. Low thermal conductivity boulder with high porosity identified on C-type asteroid (162173) Ryugu. *Nat. Astron.* **2019**, *3*, 971–976. [CrossRef]
103. Andersson, O.; Suga, H. Thermal conductivity of the Ih and XI phases of ice. *Phys. Rev. B* **1994**, *50*, 6583–6588. [CrossRef]
104. Andersson, O.; Inaba, A. Thermal conductivity of crystalline and amorphous ices and its implications on amorphization and glassy water. *Phys. Chem. Chem. Phys.* **2005**, *7*, 1441–1449. [CrossRef] [PubMed]
105. Hobbs, P.V. *Ice Physics*; Clarendon: New York, NY, USA, 1974; p. 837.
106. Lintzén, N.; Edeskär, T. Uniaxial strength and deformation properties of machine-made snow. *J. Cold Reg. Eng.* **2015**, *29*, 04014020. [CrossRef]
107. Karagianni, A.; Karoutzos, G.; Ktena, S.; Vagenas, N.; Vlachopoulos, I.; Sabatakakis, N.; Koukis, G. Elastic properties of rocks. *Bull. Geol. Soc. Greece* **2010**, *43*, 1165–1168. [CrossRef]
108. Sun, W.-J.; Kothari, S.; Sun, C.C. The relationship among tensile strength, Young's modulus, and indentation hardness of pharmaceutical compacts. *Powder Technol.* **2018**, *331*, 1–6. [CrossRef]
109. Matonti, C.; Attree, N.; Groussin, O.; Jorda, L.; Viseur, S.; Hviid, S.F.; Bouley, S.; Nébouy, D.; Auger, A.-T.; Lamy, P.L.; et al. Bilobate comet morphology and internal structure controlled by shear deformation. *Nat. Geosci.* **2019**, *12*, 157–162. [CrossRef]
110. Möhlmann, D.; Seidensticker, K.J.; Fischer, H.-H.; Faber, C.; Flandes, A.; Knapmeyer, M.; Krüger, H.; Roll, R.; Scholten, F.; Thiel, K.; et al. Compressive strength and elastic modulus at Agilkia on comet 67P/Churyumov-Gerasimenko derived from the SESAME/CASSE touchdown signals. *Icarus* **2018**, *303*, 251–264. [CrossRef]